VNU Journal of Science: Medical and Pharmaceutical Sciences, Vol. 41, No. 2 (2025) 95-107

VNU Journal of Science: Medical and Pharmaceutical Sciences

Journal homepage: https://js.vnu.edu.vn/MPS

Original Article

Anatomical Influences on Electrical Impedance Tomography: Bioimpedances in Cardiac Radiofrequency Ablation

Nguyen Minh Duc[1,2,*], Ngo Anh Huyen[1], Hoang Minh Thao[1], Nguyen Phuong Linh[1], Pierre Qian[2]

[1]*School of Electrical and Electronic Engineering, Hanoi University of Science and Technology, 1 Dai Co Viet, Hai Ba Trung, Hanoi, Vietnam*

[2]*Westmead Applied Research Centre, University of Sydney, 176 Hawkesbury Road, Westmead, NSW 2145, Australia*

Received 17th February 2025
Revised 16th May 2025; Accepted 16th June 2025

Abstract: Electrical Impedance Tomography (EIT) can potentially improve cardiac radiofrequency ablation's efficacy in treating arrhythmias, as proven in simulations and *in vivo* experiments. However, a proper EIT model for measuring ablation lesions is still absent without access to patients' CT scans in practice. This study explored the anatomical structure's influences on EIT bioimpedances to provide guidance on which organs are required for an EIT ablation model. Ablations and 64-channel bioimpedances were simulated using a realistic thoracic model built from open-source CT scans. Multiple ablation conditions and catheter locations were generated to obtain a diverse set of lesions. EIT bioimpedances were simulated under different model conditions, ranging from the simplest model containing only the heart and lungs to the full model including most major thoracic and abdominal organs. Tukey's HSD tests and differences in EIT bioimpedances were conducted to evaluate the contribution of each organ to the lesion impedances. The results showed that the thoracic bones were heavily influential and could overshadow other organs' effects. However, the inclusion of both abdominal organs and scapulae could produce a similar effect when the thoracic bones were absent. Therefore, one could choose to include either thoracic bones or abdominal organs and scapulae in the EIT model, not necessarily together, aside from the heart and lungs for lesion ablation imaging. Further *in vivo* experiments are required to test these results.

Keywords: Electrical Impedance Tomography, modeling, cardiac catheter ablation.

* Corresponding author.
E-mail address: duc.nguyenminh5@hust.edu.vn

https://doi.org/10.25073/2588-1132/vnumps.4750

1. Introduction

Arrhythmias are increasingly prevalent worldwide due to aging populations, increasing consumption of caffeine, and fast-paced lifestyles [1]. Anti-arrhythmic medications are often prescribed as the first-line treatment, but the efficacy remains modest with many side effects [2]. Pacemaker and implanted cardiac defibrillator (ICD) are supplementary devices for managing heart rhythm and preventing sudden death, but they do not treat the diseases [3]. Cardiac radiofrequency (RF) ablation is the cornerstone for arrhythmia treatments that can eliminate the arrhythmic sources and restore cardiac functions [4]. By introducing an ablation catheter into the heart via the femoral vein and releasing radiofrequency energy (~500 kHz) into the muscles that contain arrhythmic signals, the procedure aims to remove the diseased muscles permanently from the global cardiac contraction. However, the ablation success is still suboptimal and widely varied (64-85% success rate), with up to 50% of patients having to return for multiple repeated ablations due to the failure of containing the diseased muscles [5]. Numerous factors can affect ablation's efficacy (catheter-to-tissue contact, circulation, ablation power and duration, etc.), which are currently monitored via many surrogate parameters available in the catheterisation laboratory such as the circuit RF impedance, the temperature at the catheter tip, the catheter-tissue contact force and local electrogram (EMG) [4]. None of them provides a good measure of lesion formation and size growing inside the heart muscle during the ablation, which is critical to clinical decision-making and ablation success. The unavailable lesion information is one of the key reasons that minimizes the ablation efficacy.

Recently, we have demonstrated the capability of Electrical Impedance Tomography (EIT) in monitoring the lesion growth within the heart muscle during ablation. New imaging algorithms and measurement optimisation were proposed and tested *in silico*, being able to measure the lesion size within the error of 1 mm (depth) and 2.5 mm (width) [6, 7]. A hardware prototype was designed and tested in phantoms and *in vivo*, demonstrating high correlations to the lesion dimension and was superior to a current clinical method, the circuit impedance ($R2 = 0.82$ versus 0.6 on average) [8]. The system could become the first to provide real-time images of lesion information during the ablation, thus helping cardiologists to produce better judgment of the procedure and improve the ablation success.

Nonetheless, EIT modeling and imaging algorithms were not able to be deployed during *in vivo* experiments due to a critical but practical problem: the accessibility to the patient's CT scans. Depending on the ablation procedure type and the routine unique to each cardiologist, patients are not always prescribed CT scans. Unfortunately, a huge part of EIT's accuracy is to know the patient's anatomy beforehand and produce a detailed 3D body model for calculations, which can only be obtained from CT or MRI scans. For most EIT applications, detailed anatomy information of the measured object is often unavailable, so the common method is to construct one reusable model for all objects based on common anatomy knowledge, normally only including lungs (major organ influencing the body impedance) [9-11] and the organ of interest, i.e. the heart in this application [6, 7]. This approach is workable for lung monitoring, where the gas change within the lungs causes huge impedance variations that already stand out compared to other biological activities. In cardiac ablation, however, each lesion only happens in one small corner within the heart muscles, so the impedance magnitudes are more likely to be affected by the organ structures and surface electrode positions. Unfortunately, without patients' CT scans, one common model reused for all ablation procedures is inevitable, and the question is how detailed a thoracic model is required to still image the lesion within the acceptable errors. No studies have explored the effects of anatomical structure, i.e., the presence of different organs, on the lesion-related impedances to provide

more insights into building a proper EIT ablation model. This is the bottleneck for EIT imaging algorithms to be applicable in the catheterisation laboratory.

In this study, we are back to the simulations, where a realistic thoracic model with the inclusion of most major organs was built, and ablated lesions were produced at different sites using various powers and cooling conditions to investigate the influence of organ structures, lesion locations, and temperature gradients on the impedance measurements. Impedances from the catheter tip to several surface electrodes during ablations were simulated and analysed to produce guidelines for EIT modeling adjustments and to re-evaluate EIT's capability when little prior information is available.

2. Methodology

2.1. Simulation Design

The simulation design process for lesion generation and subsequent impedances is presented in Figure 1. Two thoracic models were built, one (simpler) for ablations and one (more anatomically complex) for impedance simulations. Different catheter locations in four chambers, power ablations, and convection cooling conditions were chosen to generate varied lesion sizes using COMSOL Multiphysics 5.6 (COMSOL, USA). The lesion mesh would be then overlayed into the impedance model's heart to re-mesh and the measured impedances would be simulated between the catheter tip and each pair of surface electrodes using the EIDORS tool in Matlab 2023a, a dedicated tool for EIT to simulate multichannel impedances within a 3D object and perform imaging algorithms to image the events of interest [12]. The impedances were generated under different anatomical conditions from a simple, conventional model of only lungs and heart to a complete model consisting of most major organs. Temperature formations and lesion dimensions were extracted from the ablation model as dependent variables to analyse the anatomical structures' effect on lesion-related impedances.

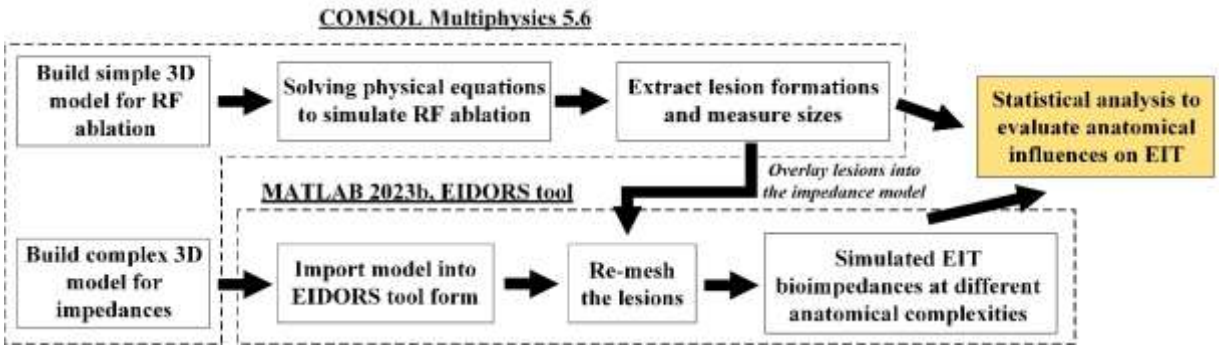

Figure 1. RF ablation and EIT bioimpedance simulation process.

2.2. Model for Ablation and Impedance Simulations

Figures 2 and 3 illustrate the two models for lesion creation and impedance simulations. The simple model for ablation, including only a heart and two lungs, is to reduce unnecessary computational resources and times, since the studies focus on the anatomical influences on the impedances, not the ablation performance. The catheter modeled the Biosense Webster Smarttouch SF catheter (Biosense Webster Inc., Diamond Bar, USA), a widely used catheter series in the cath lab with two electrodes, including the catheter tip (E1) and a follow-up electrode (E2). The RF energy will be induced between the catheter tip and a RF return pad of 6 x 12 cm on the patient's back to heat the heart

muscle. Since every 1mm increase in the lesion depth is important, it is mandatory to make an extremely fine mesh for the heart muscles to distinguish lesion sizes within 1mm resolution. However, making the whole heart a fine mesh is also redundant because the lesion only occupies a small area next to the catheter tip. As a result, the mesh was only fine (maximum element edge of 0.4 mm) within a block of 30x30mm around the catheter tip (Figure 2) where the lesion would reside, while the rest of the heart muscles were meshed in normal density.

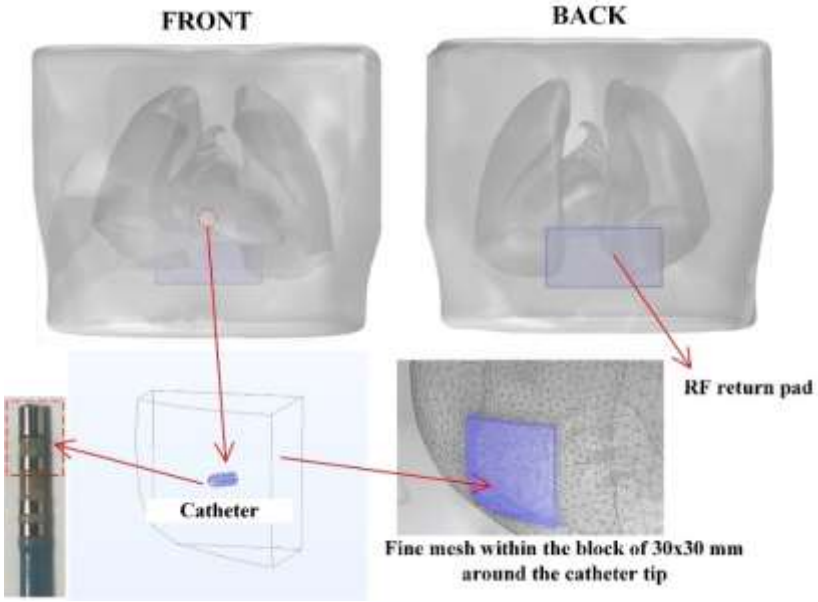

Figure 2. Model for RF ablation including only two lungs and a heart, which consists of heart muscles and chambers. An RF energy would be induced between the catheter tip inside the heart and a return pad on the back. Only the area of 30x30 mm around the catheter tip was meshed finely for the lesion creation. The catheter modelled the Biosense Webster Smarttouch SF catheter (Biosense Webster Inc., Diamond Bar, USA).

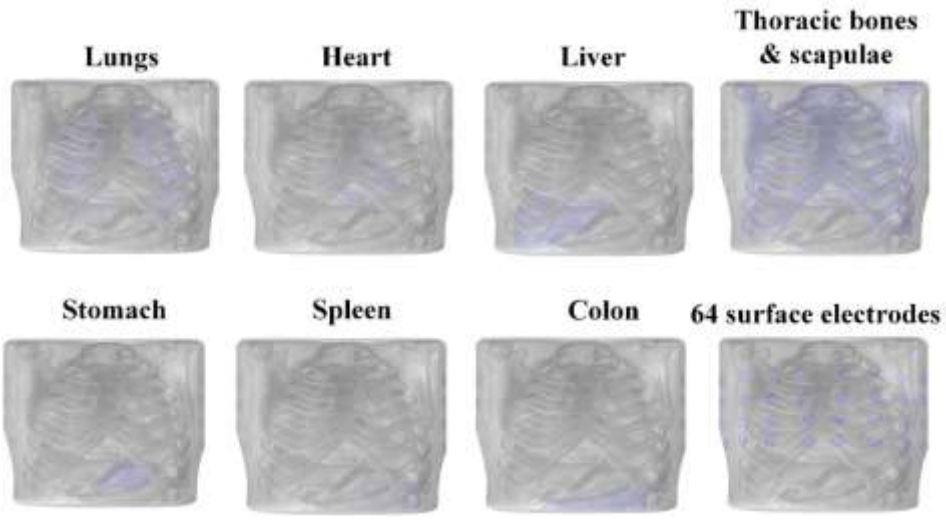

Figure 3. Model for impedance simulations containing most major organs: thoracic bones and scapula, lungs, heart, and abdominal organs. 64 surface electrodes, divided into 4 bands, were placed on the thorax.

The 3D model for impedance simulations (Figure 3) was more anatomically complex with the inclusion of thoracic bones and scapulae, lungs, heart, and abdominal organs (liver, stomach, spleen, and colon). In the latest animal experiment [8], 64 surface electrodes, divided into 4 bands, were equally spaced on the animal's thorax. The same setting was replicated in this simulation with the top band at the second rib's height and the last band at the sixth rib's height. The electrode was circular (10 mm radius).

2.3. Cardiac Ablation Simulation

The RF energy is induced around 500 kHz from the catheter tip, from which the RF current will penetrate the heart muscle and generate resistive heat near the catheter tip. The heat will then propagate into the deep tissue, with the temperature decreasing with increasing distance from the catheter [13]. The lesion is formed when a tissue is heated beyond 50 ℃ for a few seconds.

In simulation, RF ablation is the answer to solving two consecutive physical equations in the 3D model: the electrical and the thermal. At 500 kHz, the electrical conduction can be considered to be quasi-static, thus, the governing electrical equation can be simplified as:

$$\nabla \cdot (\sigma \nabla V) = 0. \quad (1)$$

Where ∇ is the gradient operator, σ and V are the conductivity distribution and the electric potential distribution within the model, respectively. The conductivities of different organs are already available in the literature [14, 15] while the RF pattern is known (between the catheter tip and the return pad), solving (1) will result in the electrical potential distribution V throughout the model. The RF source is a voltage with variable values described later to provide different ablation powers for lesion creation.

With resulted V, solving the thermal equation (Pennes' bioheat transfer [16] – equation 2) will convert V into the thermal damage from which the lesion zone is defined. In practice, the thermal damage almost stays within the heart muscles, while the irrigation from the ablation system and blood circulation will cool down any heat extending beyond of endocardium. Sometimes, the heat can go beyond the epicardium, leading to potential complications, but they are not the focus of this study. Therefore, the thermal equation is only applied within the heart muscle and described as follows:

$$\rho_{myo} C_{myo} \frac{\partial T}{\partial t} = \nabla \cdot \left(k_{myo} \nabla T\right) + \nabla \cdot (\sigma_{myo}(T) \nabla V \quad (2)$$

With ρ_{myo}, C_{myo}, k_{myo}, and $\sigma_{myo}(T)$ are the density (kg/m^3), specific heat capacity ($J/kg \cdot K$), thermal conductivity ($W/m \cdot K$) and temperature-dependent conductivity (S/m, increase 2% per 1 ^oC [17]) of the myocardium.

The convection cooling effect on the endocardial surface, caused by blood circulation and irrigations, is calculated as a boundary condition:

$$-\mathbf{n} \cdot \nabla \cdot (\sigma_{myo}(T) \nabla V = q_0, \quad (3)$$

With $q_0 = h \cdot (T_{blood} - T)$, h is the blood's heat transfer coefficient that has been reported to range from 44 to 2500 ($W/m^2 \cdot K$) [18, 19]. Solving equations 2 and 3 will result in the temperature distribution within the cardiac muscles with its decreasing gradient when moving further away from the catheter (Figure 4).

The equations 1-3 were solved on the 3D model using Finite Element Method (FEM). Table 1 presents electrical (at 500 kHz) and thermal properties of different organs for ablation simulation.

In this study, a total of 13 catheter positions across all chambers were generated (Figure 4) with two catheter contact conditions for each position: being perpendicular to the endocardium and lying along the endocardium. A period of 60 seconds was repeated for all ablations, with the tissue temperatures updated every 1 second. The lesion boundary was defined at 50 ℃, and its depth and width were measured for analysis.

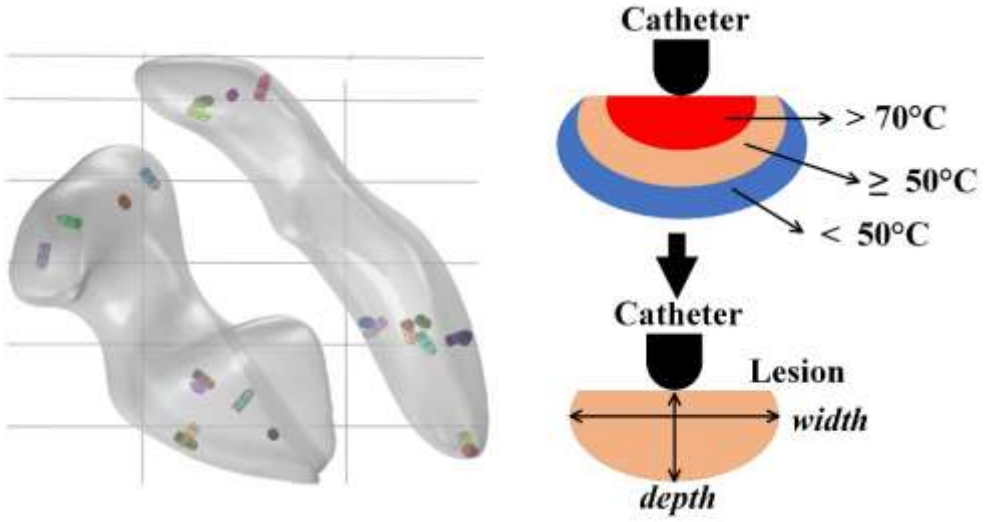

Figure 4. Catheter positions and lesion formation. Right: 16 catheter positions with 2 catheter contact conditions in each position were generated. Left: Lesion boundary defined at ≥ 50 ℃, and its depth and width were measured.

Table 1. Electrical (500 kHz) and thermal properties of blood and myocardium for ablation simulations

Organ	Electrical properties (500 kHz)		Thermal properties		
	Conductivity (S/m)	Relative permittivity	Heat capacity (J/kg.K)	Density (kg/$\mathbf{m^3}$)	Thermal conductivity (W/m.K)
Blood	0.7	5200	4180	1000	0.543
myocardium	0.28	3260	1063	3200	0.5367

2.4. EIT Multichannel Bioimpedance Simulation

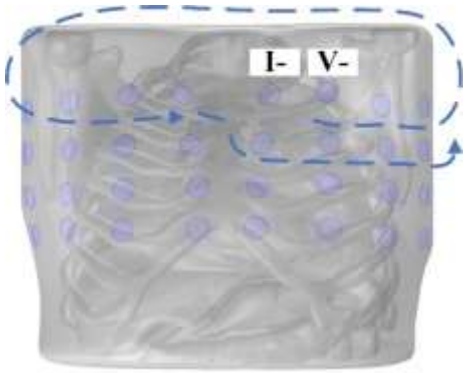

Figure 5. Each impedance channel was measured by injecting current between the catheter tip (I+) and a surface electrode (I-), and recording voltage between the catheter E2 (V+) and another surface electrode (V-) on the right of the injected one. All pairs of 64 electrodes were shuffled for impedance measurements following the arrow directions.

The EIT bioimpedance simulation was done solving a similar electrical equation to (1) except using a 4-terminal topology: a current source applied between the catheter tip (I+) and one surface electrode (I-), and a voltage recorded between the catheter electrode E2 (V+) and the adjacent surface electrode (V-) to the right of the I- one (Figure 5). By applying the current source, solving equation (1) will result in the voltage distribution V within the object and, consequently, the voltages picked up at surface electrodes. The impedance would be converted using Ohm's law:

$$Z = \frac{V_+ - V_-}{I_+ - I_-} \qquad (4)$$

The current source and voltage recording were shuffled between each pair of surface electrodes until all 64 electrodes were used, from which a set of 64 impedances was derived.

The lesion-related impedances were calculated in differential values between the baseline impedances at time 0 before the ablation started and the during-ablation impedances after the tissue temperatures were updated:

$$\Delta Z(n)_{lesion} = Z(n)_{baseline\ at\ t_0} - Z(n)_{ablation} \quad (5)$$

With n being the channel number, which ranges from 1 to 64. The EIT differential imaging using differential impedances in equation (5) was widely used in biomedical applications due to the fact that it significantly reduces the dependency on the anatomy structure, which varies from patient to patient, and instead only presents the differential impedances related to the event of interest [20]. Nonetheless, the anatomical dependency is still considerable in the EIT differential method, one of the reasons explaining the shortcomings of EIT's accuracy, especially in applications where the event of interest is small and detailed, as in cardiac ablation.

The bioimpedance simulations were solved using FEM on the model provided in Figure 3. The electrical properties of different organs were provided in Table 2 at 50 kHz, the widely used EIT frequency in clinical applications. The blood conductivity was used for any intra-space areas between organs and within the heart chambers as the baseline conductivity.

Table 2. Electrical properties at 50 kHz of different organs for EIT bioimpedance simulations

Organ	Conductivity (S/m)	Relative permittivity
Blood	0.7	5200
Myocardium	0.195	17000
Bones	0.003	181
Lung	0.1	4270
Colon	0.244	4610
Liver	0.072	10700
Spleen	0.118	5490
Stomach	0.534	3550

As described above, the multichannel bioimpedances would be simulated at different anatomical complexities using only one full model in Figure 3. The idea was to just "turn off" the organs that we wanted to exclude by assigning blood conductivity to their areas, i.e., the boundaries are there, but the impedances return to the baseline. In that manner, two bioimpedance simulation scenarios were made: i) With thoracic bones; and ii) Without thoracic bones. Within each case, different sub-cases were simulated, including full inclusion of all organs (most complex), only lungs and heart (simplest form), and other cases where each organ was "turned off" except for lungs and heart. The purpose is to i) Study the influence of thoracic bones, a high resistant organ covering most of the thorax and likely affect the impedance paths but is structurally complicated for computation, on the existence of other organs in bioimpedances; and ii) The influence of abdominal organs and scapula on the bioimpedances compared to the simplest model of just lungs and heart. Two impedance parameters were included in the statistical analysis, including the average and the maximum differential impedances:

$$\overline{\Delta Z}_{lesion} = \frac{1}{64}\sum \Delta Z(n)_{lesion} \quad (6)$$

$$\widehat{\Delta Z}_{lesion} = \max(\Delta Z(n)_{lesion}) \quad (7)$$

2.5. Statistical Analysis

Tukey's Honestly Significant Difference (HSD) test was used with $\alpha = 0.05$ on the average and maximum lesion differential impedances within different groups of anatomical scenarios to separate the groups that are statistically different from others. Significant Tukey's HSD results would confirm the importance of firstly, the thoracic bones, and secondly, each organ when the thoracic bones were absent in EIT lesion impedances.

Based on Tukey's results, the statistically significant models of the same sub-cases were selected, and the impedance data for each increment of 1mm lesion depth and 2 mm width were calculated and compared between models across the two scenarios (with and without thoracic bones). The data would be presented in

differences to evaluate in detail how serious the absence of each organ is and how many errors it could contribute to the lesion size across all size ranges.

3. Results and Discussion

3.1. Ablation Results

Table 3. Number of created lesions for each increment of 1mm in lesion depth

Lesion depth (mm)	Number of created lesions
0-1	28
1-2	497
2-3	553
3-4	889
4-5	840
5-6	1190
6-7	518
7-8	392
8-9	231
9-10	14

There were 5152 lesions generated from 13 locations and 2 catheter contact conditions. Table 3 presents the number of lesions for each increment of 1mm in lesion depth, showing the majority being within 1-9mm depth. Only a few lesions were less than 1mm or more than 9mm in depth. The < 1 mm depth is hardly a lesion to be considered because it is too small even compared to the thin atrial wall of 2-4 mm [21], while > 9 mm depth also rarely happens in practice because, more often than not, the tissue temperature has become too hot at about 7 mm to continue. A large portion of the created lesions were from 2 to 7 mm, which reflects the normal range recorded in real catheterisation laboratories around the world [22].

3.2. Anatomical Structure Effect on EIT Bioimpedances

Table 4 presents Tukey's HSD results in the same sub-cases between the with- and without-thoracic bone models. Interestingly, significant differences were only observed in the simplest model of only heart and lungs, and in the models where the scapula was removed (both $p < 0.05$), while no significant differences were reported in other paired models. The results show that the inclusion of thoracic bones was not always necessary but was situation-dependent.

Table 4. Tukey's HSD results between the with- and without-thoracic bone models

Pairs	EIT bioimpedances			
	Average value $\overline{\Delta \boldsymbol{Z}}_{\boldsymbol{lesion}}$		Maximum value $\widehat{\Delta \boldsymbol{Z}}_{\boldsymbol{lesion}}$	
	Mean difference	p	Mean difference	p
All organs	0.93	0.34	0.92	0.35
Only heart & lungs	-4.08	< 0.05	-4.04	< 0.05
No liver	0.94	0.34	0.93	0.35
No colon	0.93	0.34	0.92	0.35
No stomach	0.92	0.35	0.93	0.35
No spleen	0.92	0.34	0.92	0.35
No scapula	-4.09	< 0.05	-4.06	< 0.05

In the only lungs and heart models, the inclusion of thoracic bones did change the lesions' differential impedances, proving that this simple but common model for other EIT applications should not be employed in cardiac ablation. However, when the abdominal organs were included in the model, the thoracic bones altered EIT impedances much less significantly. It is also applied to the abdominal organs, "turning off" each of the organs has no meaningful impact on EIT impedances as long as other organs are still "on". The scapula models are an interesting case, potentially because the scapulae are also bones with similar high impedance but do not cage other organs like the thoracic bones do. When the thoracic bones

were included, the impedance paths were already blocked around the scapula regions, so the scapulae's effect was negligible. In other words, the scapulae's influence on EIT impedances was only significant when the thoracic bones were excluded. It could also be because the scapula is positioned on the back away from other abdominal organs, therefore, it influences certain EIT impedance paths that go to the back surface electrodes.

Another noticeable result was that similar t-values and p-values were reported for both the average and maximum values out of 64 EIT bioimpedances. This shows the anatomical structure affected both parameters equally, which is a good thing for the EIT model, not concern individual measurements when building a model.

Looking at the Tukey's HSD results in Table 4 between different pairs of models within each scenario (with and without thoracic bones), no statistical significance was found in any pairs when there were thoracic bones. These extreme results indicate the heavy influence of the thoracic bones in the EIT model, such that they overshadow any organs' impacts on the EIT impedances. Table 5 presents Tukey's HSD test results in the second scenario (without thoracic bones), exhibiting a more complex picture. Either compared to the simplest model (only heart and lungs) or the full model, the scapula's "on" and "off" affected significantly the lesions' impedances, enforcing the idea that scapulae were indeed important in the absence of the thoracic bones. Meanwhile, the inclusion of abdominal organs into the simplest model would also affect the lesion's impedances regardless of organ type. However, no significance was found when comparing the two models that excluded different abdominal organs, even though they had considerably different conductivities from high (spleen) to low (liver) (Table 2). This showed that the abdominal organs as a whole acted as an obstruction to EIT impedances, but each organ's influence was minuscule within the whole region.

Table 5. Tukey's HSD results on each pair of models in the without-thoracic-bones scenario

Pairs of models		EIT bioimpedances			
		Average value $\overline{\Delta \boldsymbol{Z}}_{\boldsymbol{lesion}}$		Maximum value $\widehat{\Delta \boldsymbol{Z}}_{\boldsymbol{lesion}}$	
Model 1	Model 2	Mean difference	p	Mean difference	p
Full	Heart & lungs	-4.82	< 0.05	-4.84	< 0.05
Full	No colon	0.01	0.99	-0.01	0.99
Full	No liver	0.14	0.99	0.12	0.99
Full	No scapulae	-4.96	< 0.05	-4.96	< 0.05
Full	No spleen	0.01	0.99	0.01	0.99
Full	No stomach	0.03	0.99	0.02	0.99
Heart & lungs	No colon	4.82	< 0.05	4.84	< 0.05
Heart & lungs	No liver	4.96	< 0.05	4.96	< 0.05
Heart & lungs	No scapulae	-0.14	0.99	-0.12	0.99
Heart & lungs	No spleen	4.82	< 0.05	4.84	< 0.05
Heart & lungs	No stomach	4.83	< 0.05	4.84	< 0.05
No scapulae	No spleen	4.96	< 0.05	4.97	< 0.05
No scapulae	No stomach	4.97	< 0.05	4.98	< 0.05
No colon	No liver	0.13	0.99	0.12	0.99
No colon	No scapulae	-4.97	< 0.05	-4.96	< 0.05
No colon	No spleen	-0.01	0.99	0.01	0.99
No colon	No stomach	0.02	0.99	0.01	0.99
No liver	No scapulae	-5.10	< 0.05	-5.08	< 0.05
No liver	No spleen	-0.14	0.99	-0.12	0.99
No liver	No stomach	-0.14	0.99	-0.12	0.99
No spleen	No stomach	0.01	0.99	0.01	0.99

3.3. EIT Bioimpedances Between Models in Different Lesion Size Ranges

Figure 6 illustrate the differences in mean impedances in each increment of 1mm depth and 2 mm width between with- and without-thoracic bones scenarios in three models: i) Full inclusion of all organs; ii) Only heart and lungs; and iii) No scapulae, with the two latter models being shown to be statistically differences in the previous section. The mean impedance differences were mostly small (< 3Ω) in the full models in both lesion depth and width, except for the 8-9 mm depth range and the 8-12 mm width range. Meanwhile, the differences were consistently significant in the other two models in lesion depth (3-11Ω) and width (3-14Ω). This confirms that the thoracic bones' effect was minimised when there were other organs present (low impedance differences in the full models compared to high differences in the simple models of only heart and lungs). The results also indicated the importance of the scapulae in the model if the thoracic bones were absent. Most importantly, Figure 6 showed relatively equal influences of the anatomical differences across all lesion depth ranges, the most important parameter to consider whether the ablation is successful (transmural lesion) or not (non-transmural) [4]. Similar results were also reported in the differences of maximum impedances (therefore not shown here).

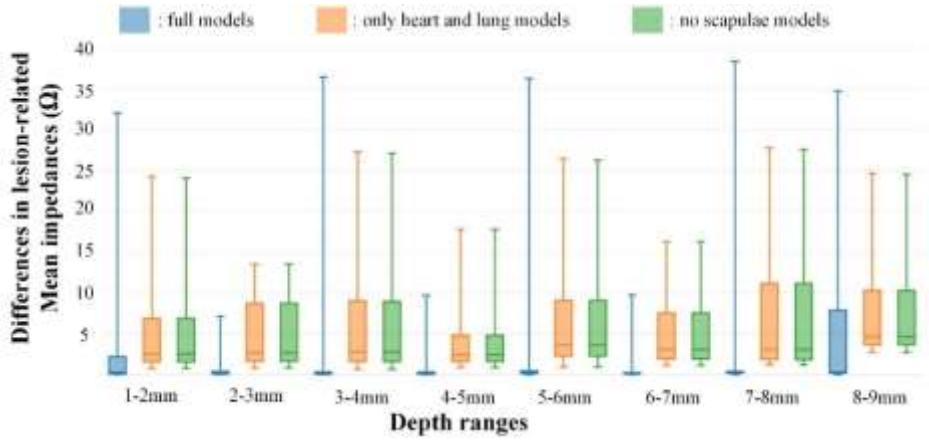

(A)

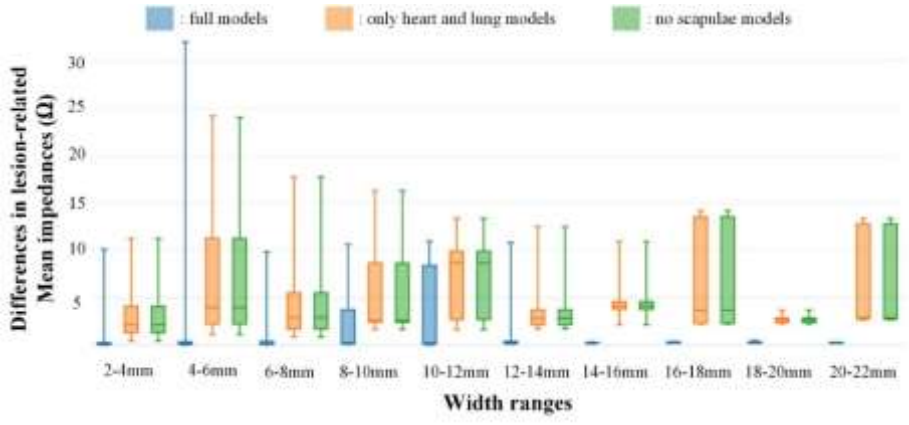

(B)

Figure 6**.** Differences in mean impedances between with- and without-thoracic bones scenarios in 3 three models: full, only heart and lungs, and no scapulae in varied lesion depth (A) and width ranges (B).

Table 6 presents the lesion impedances per 1 mm depth and width calculated for each depth and width range using the full model with thoracic bones. The bigger the lesion is in both depth and width axes, the more sensitive the impedances are to the lesion growth, i.e., a smaller impedance change can lead to a higher increment in lesion depth and width at higher ranges. From Figure 6, ones can see that 3-11Ω (lesion depth) and 3-14Ω (lesion width) discrepancies in the two models of only heart and lungs and no scapulae can lead to errors of 1-2 mm and 1-3 mm for the lesion depth and width respectively at the middle to high lesion ranges. Such errors are only model-related and do not yet account for other errors from instruments and physiological activities (cardiac and respiratory cycles), emphasising the importance of picking the right EIT model as the first step toward imaging lesion growth during ablation.

. Table 6. The impedance changes per 1 mm depth and 1 mm width, calculated from the full model with the thoracic bones

Depth ranges (mm)	$\Delta Z_{lesion}/1mm\ depth$	Width ranges (mm)	$\Delta Z_{lesion}/1mm\ width$
1-2	14.8 ± 7.4	2-4	9.5 ± 4.8
2-3	12.7 ± 6.2	4-6	6.1 ± 3.6
3-4	9.0 ± 5.2	6-8	4.7 ± 2.3
4-5	8.1± 4.3	8-10	4.7 ± 1.9
5-6	6.9 ± 3.2	10-12	4.4 ± 1.7
6-7	6.7 ± 2.5	12-14	3.1 ± 0.4
7-8	6.4 ± 3.2	14-16	3.7 ± 0.8
8-9	5.6 ± 1.5	16-18	3.8 ± 2.1
		18-20	2.3 ± 0.2
		20-22	3.1 ± 1.5

3.4. Summarisation of Key Findings

The study's key findings can be summarised as follows:

i) The simple but common EIT model, which consists of only the heart and lungs, used in many other EIT applications, cannot be replicated in cardiac ablation, which requires a higher standard to achieve desirable accuracy;

ii) The thoracic bones influence EIT impedances heavily and can overshadow other organs' effects, meaning thoracic bones' inclusions with the lungs and heart might be enough. However, thoracic bones are also very difficult to mesh and will significantly increase the computation time;

iii) If the thoracic bones are not considered, one needs to include the scapulae and abdominal organs in the EIT model. However, abdominal organs can be combined as one region under the lungs, which has a similar effect to constructing individual organs. Scapulae are also easier to simplify compared to the thoracic bones, as they only cover some areas in the back.

In short, there are two relatively equal options for EIT models to develop imaging algorithms for cardiac ablations, including either: i) the lungs, heart, and thoracic bones, or ii) the lungs, heart, abdominal organs (but can be grouped as one big object), and scapulae.

3.5. Study Limitations

The first study limitation is the absence of fatty tissues, which vary significantly from patient to patient. Fatty tissues also have a high impedance, potentially adding more anatomical complexity to EIT impedances. Nonetheless, unlike the thoracic bones, which cage other organs inside but are much more complicated in shape with lots of spaces in between, fatty tissues can be guaranteed to fill everywhere under the

thoracic skin in patients who have to undergo ablations. Thus, the impedance blockages are likely evenly distributed around the thorax, making the differential EIT method the ideal solution to subtract the fatty impedances from the equations.

The second limitation is the nature of tissues' inhomogeneity in the electrical properties, i.e., the tissue impedance is directional and not the same across the whole organ. This is a common issue in EIT simulations, and its effect can only be found via *in vivo* experiments, which will be conducted using the EIT model results from this study.

Finally, the study did not incorporate patient motions in the modelling, which has been known to considerably shift electrode positions and influence EIT measurements. The body movements lead to a mismatch between the EIT model and the measured object, thus creating uncertainties and artifacts in the image reconstruction process. Some studies found that chest movements can contribute up to 18.31% to the thoracic impedances [23, 24]. However, general anesthesia is commonly administered to patients undergoing catheter ablation procedures, which helps minimize motion artifacts during the procedure. This approach effectively stabilizes patient movements, allowing for more accurate and reliable recordings. In a prior animal study [8], multichannel bioimpedance signals were synchronized with both respiratory and cardiac cycles to obtain stable recordings, thereby establishing a methodological framework for similar applications in future research.

4. Conclusion

This study explored in detail the anatomical structure's influence on EIT bioimpedances in cardiac ablation, which allows other studies to pick the right model to image the lesion growth during the ablation. The study performed ablation and multi-channel impedance simulations on a thoracic model built from open-source CT scans, including most major organs that could influence lesion-related impedances. Multiple ablation lesions at different ablation conditions and catheter locations inside the heart were created, and the effect of each organ on lesion-related EIT bioimpedances was thoroughly studied. The results indicated that the thoracic bones can heavily influence the impedances with or without other organs, but can be substituted with the abdominal organs and scapulae in the model to provide equal blockages to EIT bioimpedances. Therefore, it is up to researchers to pick which option to go for in order to build a proper EIT ablation model. Further *in vivo* experiments will be required to test the results and will be conducted in the near future.

Acknowledgement

This research is funded by Vietnam National Foundation for Science and Technology Development (NAFOSTED) under grant number 108.99-2021.44.

References

[1] G. Lippi, F. S. Gomar, G. Cervellin, Global Epidemiology of Atrial Fibrillation: an Increasing Epidemic and Public Health Challenge, International Journal of Stroke, Vol. 16, No. 2, 2021, pp. 217-221, https://doi.org/10.1177/1747493019897870.

[2] Z. U. A. Asad et al., Catheter Ablation versus Medical Therapy for Atrial Fibrillation: a Systematic Review and Meta-Analysis of Randomized Controlled Trials, Circulation: Arrhythmia and Electrophysiology, Vol. 12, No. 9, 2019, pp. e007414, https://doi.org/10.1161/CIRCEP.119.007414.

[3] B. Blanch et al., Implantable Cardioverter–Defibrillator Therapy in Australia, 2002–2015, Medical Journal of Australia, Vol. 209, No. 3, 2018, pp. 123-129, https://doi.org/10.5694/mja17.01183.

[4] H. Calkins et al., Hrs/Ehra/Ecas/-Aphrs/Solaece Expert Consensus Statement on Catheter and Surgical Ablation of Atrial Fibrillation, EP Europace, Vol. 20, No. 1, 2018, pp. e1-e16, https://doi.org/10.1093/europace/eux274.

[5] F. Holmqvist et al., A Decade of Catheter Ablation of Cardiac Arrhythmias in Sweden: Ablation

Practices and Outcomes, European Heart Journal, Vol. 40, No. 10, 2019, pp. 820-830, https://doi.org/10.1093/eurheartj/ehy709.

[6] D. M. Nguyen, P. Qian, T. Barry, A. McEwan, The Region-of-Interest Based Measurement Selection Process for Electrical Impedance Tomography in Radiofrequency Cardiac Ablation with Known Anatomical Information, Biomedical Signal Processing and Control, Vol. 56, 2020, pp. 101706, https://doi.org/10.1016/j.bspc.2019.101706.

[7] D. M. Nguyen, P. Qian, T. Barry, A. McEwan, Self-Weighted NOSER-Prior Electrical Impedance Tomography using Internal Electrodes in Cardiac Radiofrequency Ablation, Physiological Measurement, Vol. 40, No. 6, 2019, pp.065006, https://doi.org/10.1088/1361-6579/ab1937.

[8] P. C. Qian et al., Optimizing Impedance Change Measurement during Radiofrequency Ablation Enables More Accurate Characterization of Lesion Formation, Clinical Electrophysiology, Vol. 7, No. 4, 2021 pp. 471-481, https://doi.org/10.1016/j.jacep.2020.09.011.

[9] A. Adler, M. B. Amato, J. H. Arnold et al., Whither Lung EIT: Where are We, Where do We Want to Go and What do We Need to Get There?, Physiological Measurement, Vol. 33, No. 5, 2012, pp. 679, https://doi.org/10.1088/0967-3334/33/5/679.

[10] G. Y. Jang et al., Integrated EIT System for Functional Lung Ventilation Imaging, Biomedical Engineering Online, Vol. 18, No. 1, 2019, pp. 83, https://doi.org/10.1186/s12938-019-0701-y.

[11] Y. Shi, Z. Yang, F. Xie, S. Ren, S.F. Xu, The Research Progress of Electrical Impedance Tomography for Lung Monitoring, Frontiers in Bioengineering and Biotechnology, Vol. 9, 2021, pp. 726652, https://doi.org/10.3389/fbioe.2021.726652.

[12] M. Vauhkonen, W. R. Lionheart, L. M. Heikkinen, P. J. Vauhkonen, J. P. Kaipio, A Matlab Package for the Eidors Project to Reconstruct Two-Dimensional EIT Images, Physiological Measurement, Vol. 22, No.1, 2001, pp. 107, https://10.1088/0967-3334/22/1/314.

[13] S. Ernst, Catheter Ablation: General Principles and Advances, Cardiac Electrophysiology Clinics, Vol. 9, No. 2, 2017, pp. 311-317, https://doi.org/10.1016/j.ccep.2017.02.012.

[14] N. Gallagher, E.C. Fear, I. A. Byrd, E. J. Vigmond, Contact Geometry Affects Lesion Formation in Radiofrequency Cardiac Catheter Ablation, PloS One, Vol. 8, No. 9, 2013, pp. e73242, https://doi.org/10.1371/journal.pone.0073242.

[15] C. Gabriel, S. Gabriel, Compilation of the Dielectric Properties of Body Tissues at RF and Microwave Frequencies, Report N.AL/OE-TR-1996-0037, Occupational and Environmental Health Directorate, Radiofrequency Radiation Division, Brooks Air Force Base, Texas (USA), 1996.

[16] C. K. Charny, Mathematical Models of Bioheat Transfer, Advances in Heat Transfer, Vol. 22, 1992, pp. 19-155, https://doi.org/10.1016/S0065-2717(08)70344-7.

[17] E. Gersing, Monitoring Temperature-Induced Changes in Tissue during Hyperthermia by Impedance Methods A, Annals of the New York Academy of Sciences, Vol. 873, No. 1, 1999, pp. 13-20, https://10.1111/j.1749-6632.1999.tb09444.x.

[18] D. Schutt, E. J. Berjano, D. Haemmerich, Effect of Electrode Thermal Conductivity in Cardiac Radiofrequency Catheter Ablation: a Computational Modeling Study, International Journal of Hyperthermia, Vol. 25, No. 2, 2009, pp. 99-107, https://10.1080/02656730802563051.

[19] A. G. Suárez, F. Hornero, E. J. Berjano, Mathematical Modeling of Epicardial RF Ablation of Atrial Tissue with Overlying Epicardial Fat, The Open Biomedical Engineering Journal, Vol. 4, 2010, pp. 4, https://doi.org/10.2174/1874120701004020047.

[20] B. Brazey, Y. Haddab, N. Zemiti, Robust Imaging using Electrical Impedance Tomography: Review of Current Tools, Proceedings of the Royal Society A, Vol. 478, No. 2258, 2022, pp. 20210713, https://10.1098/rspa.2021.0713.

[21] J. Whitaker et al., The Role of Myocardial Wall Thickness in Atrial Arrhythmogenesis, EP Europace, Vol. 18, No. 12, 2016, pp. 1758-1772, https://10.1093/europace/euw014.

[22] F. Bourier et al., High-Power Short Duration versus Standard Radiofrequency Ablation: Insights on Lesion Metrics, Journal of Cardiovascular Electrophysiology, Vol. 29, No. 11, 2018, pp. 1570-1575, https://10.1111/jce.13724.

[23] J. Zhang, R. P. Patterson, EIT Images of Ventilation: What Contributes to the Resistivity Changes?, Physiological Measurement, Vol. 26, No. 2, 2005, pp. 81-92, https://doi.org/10.1088/0967-3334/26/2/008.

[24] A. Adler, R. Guardo, Y. Berthiaume, Impedance Imaging of Lung Ventilation: Do We Need to Account for Chest Expansion?, IEEE Transactions on Biomedical Engineering, Vol. 43, No. 4, 1996, pp. 414-420, https://doi.org/10.1109/10.486261.